Journal of Magnetic Resonance 208 (2011) 136–147

Contents lists available at ScienceDirect

Journal of Magnetic Resonance

journal homepage: www.elsevier.com/locate/jmr

Design and applications of an *in situ* electrochemical NMR cell

Xiaocan Zhang, Josef W. Zwanziger *

Department of Chemistry, Dalhousie University, Halifax, Nova Scotia, Canada B3H 4J3

ARTICLE INFO

Article history:
Received 4 August 2010
Revised 21 October 2010
Available online 27 October 2010

Keywords:
Electrochemistry
Solution NMR

ABSTRACT

A device using a three-electrode electrochemical cell (referred to as an ECNMR cell) was successfully constructed that could be used in a standard 5 mm NMR probe to acquire high-resolution NMR spectra while the working electrode was held at a constant electrical potential. The working electrode was a 20 nm thick gold film thermally coated on the outside of an inner 3 mm glass tube. An underlayer consisting of (3-mercaptopropyl)trimethoxy-silane was coated on the glass surface in order to improve its adhesion to gold. Tests showed prolonged life of the gold film. Details of the design and construction of the ECNMR cell are described. The ECNMR cell could be routinely used in a multi-user service high-resolution NMR instrument under oxygen-free conditions in both aqueous and non-aqueous solvents. Different approaches were applied to suppress the noise transmitted between the potentiostat and the NMR spectrometer. These approaches were shown to be effective in reducing background noise in the NMR spectra. The electrochemical and NMR performance of the ECNMR cell is presented. The reduction of 1,4-benzoquinone in both aqueous and non-aqueous solvents was used for testing. The evolution of the *in situ* ECNMR spectra with time demonstrated that use of the ECNMR cell was feasible. Studies of caffeic acid and 9-chloroanthracene using this ECNMR cell were undertaken to explore its applications, such as monitoring reactions and studying their reaction mechanisms.

1. Introduction

Electrochemical nuclear magnetic resonance spectroscopy (ECNMR) involves performing electrochemistry directly in a high-resolution NMR probe. It is very powerful in obtaining *in situ* quantitative structural and mechanistic characterization of a chemical system. More information is obtained by conducting simultaneous electrochemical and spectrometric experiments rather than by performing each experiment separately. However, the realization of an *in situ* ECNMR probe encounters conflicting requirements between electrochemistry and NMR spectroscopy. On the one hand, the asymmetric, metallic electrodes and the presence of current generate inhomogeneity of the magnetic field and cause a loss in resolution and sensitivity in the NMR experiment. On the other hand, the confined NMR tube size restricts the electrochemical reaction to occur in an extremely limited space, which might distort the acquired voltammogram.

A flow cell arrangement [1,2] avoids the inherent incompatibility between electrochemistry and NMR; however, it is not truly *in situ* as the electrochemical reaction occurs outside the NMR radio frequency (rf) region. Both experimental arrangements described in the literature required a large solution volume and might not exclude oxygen during experimentation. Moreover, as the NMR detection was performed a certain time after the generation of new products, use of the method for kinetic and mechanistic studies was limited.

In situ studies have been performed by directly locating bulk electrodes inside the rf regions of an NMR probe, with varying degrees of success [3–5]. Considerable work has also been performed on solid samples, where sample size limitations are severe but high-resolution spectra are not expected [6–8]. Significant progress toward combining the electrochemical and high-resolution NMR techniques has been realized by taking advantage of the "skin depth" [9] of the electrode materials. The skin depth δ defines the thickness of a conductor over which the amplitude of the incident rf radiation falls to $1/e$ (about 37%) of its original value. In mathematical form, it is $A_f/A_i = \exp(-d/\delta)$, where A_i and A_f are the initial and final amplitude of the rf radiation, respectively, and d is the thickness of the conductor. The skin depth of a specific conducting material can be calculated from

$$\delta = \sqrt{\frac{\rho}{\pi \nu \mu_\circ}}, \tag{1}$$

where ρ is the electrical resistivity of the material (units of Ω m), ν is the rf field frequency (s^{-1}), and $\mu_\circ$ is the magnetic permeability ($H\ m^{-1}$) [9]. Bloembergen [10] studied the relation between the magnetic and conduction loss, and found that the rf field can penetrate a conducting sample without attenuation or phase shift as long as the sample dimension is small compared to the skin depth.

* Corresponding author.
E-mail address: jzwanzig@dal.ca (J.W. Zwanziger).

1090-7807/$ - see front matter © 2010 Elsevier Inc. All rights reserved.
doi:10.1016/j.jmr.2010.10.013

A thin metal film has been used by several research groups [11–13] as a working electrode to take advantage of the skin depth effect in an *in situ* ECNMR cell. Mincey et al. [11] used an Sb–SnO_2 semiconductor film as the working electrode; Prenzler et al. [12] and Webster [13] both used gold films as working electrode. The gold film electrode is metallic and provides a faster electrolysis rate than the Sb–SnO_2 semiconductor film. However, both gold film systems [12,13] used a 10 mm or larger size NMR tubes. Very recently, Dunsch et al. [14] used large scale carbon fibers for both working and counter electrodes. The metal-free electrodes were unique in producing an enhanced homogeneity of the NMR magnetic field. Nevertheless, a 75% decrease of the signal-to-noise ratio and a four-times-broadening of signals were reported. This profound weakness in NMR signal might have been due to the high current (*i.e.*, over 28,000 times more than a conventional platinum electrode system) generated by the large scale electrode. Therefore, it is debatable whether the large scale electrodes are advantageous in the NMR performance.

This paper presents the design and applications of a 5 mm ECNMR cell, a particularly common size in modern liquid-phase NMR, with a thin gold film as the working electrode. The lab-built ECNMR cell is capable of studies in both aqueous and non-aqueous solutions. To validate the design and approach, results are presented on the reduction of benzoquinone in both aqueous and non-aqueous solvents. Then, two brief applications are presented, on the oxidation of caffeic acid and the reduction of 9-chloroanthracene.

2. Experimental

All chemicals used were reagent grade and included 1,4-benzoquinone ($\geqslant$99.5%, Fluka), 9-chloroanthracene (96.0%, Aldrich), anthracene (96.0%, Sigma–Aldrich), Bu_4NPF_6 (98%, Aldrich) and acetonitrile (HPLC, Fisher). Caffeic acid ($\geqslant$99.0%) was purchased from Fluka. Deionized water was purified with a hydro-purification system connected in series to a Millipore Direct-Q®3 system. In NMR studies, acetonitrile-d_3 (99.8 atom%D, Aldrich) was used to prepare deuterated solutions.

All electrochemical measurements were performed by a computer-controlled, lab-built potentiostat with home-written software. The sweep rate was 100 mV s^{-1} unless otherwise stated. Background runs were performed and subtracted from the reported cyclic voltammograms. All experiments were carried out at least three times with a freshly prepared solution. ^{1}H NMR spectra were acquired with a Bruker/Tecmag AC-250 Spectrometer. In order to obtain the optimum NMR performance with a limited numbers of scans, the spectra were centered at the mid-point of the proton peaks and the width of the new spectral window was set just to cover the spectra of protons of interest. The number of acquisition points was also modified in order to keep the acquisition time reasonable (*i.e.*, no greater than 2 min). In the final reported spectra, the chemical shifts were realigned to use TMS as a reference.

2.1. Design of the ECNMR cell

2.1.1. Working electrode

A thin gold film-coated on glass was used as the working electrode. As gold is known to be weakly bonded to regular glass, a underlayer was applied to improve the adhesion between the gold film and the glass substrate. (3-Mercaptopropyl)trimethoxy-silane (MPS) has been reported [15,16] to improve the adhesion due to its unique structure. The silane group could bind to an oxygen surface atom through a siloxane bond and the thiol functional group could bind strongly to the gold coating layer [17]. Only a very thin layer (*e.g.*, single molecular layer) is necessary to improve the glass surface adhesion to gold.

All glass tubes were thoroughly cleaned prior to coating. To remove organic contaminates from the surface, the glassware was first soaked in HNO_3/H_2O (50/50) for 30 min. After rinsing with deionized H_2O, they were immersed in a freshly prepared piranha solution (70% H_2SO_4/30% H_2O_2, 3:1 in volume) for 30 min before being extensively cleaned with deionized H_2O at 60 °C. All glassware was subsequently dried under a N_2 stream and ready for future use.

The following procedures [17] were used to provide a thin layer of MPS undercoating. The solution for silanization was prepared by mixing 9.5 ml of MPS (Aldrich, 95%), 10 ml of H_2O (deionized) and 510 ml of 2-propanol (VWR, 99.5%). Cleaned glass tubes were placed in the prepared silanization solution, which was subsequently brought to reflux. The area to be coated with gold was kept immersed in solution for 15 min after reaching the refluxing point. The outside surface of the glass tubes was then rinsed with 2-propanol and the inside was cleaned with a brush. This was done to remove all unwanted MPA on the inside surface. After blow drying with a jet of N_2, these tubes were gently placed in a drying oven at 100 °C for 15 min. This curing step concluded the MPS treatment of all 3 mm glass tubes.

A thin gold film was then thermally coated on top of the MPS layer on the outside of a 3 mm glass tube as the working electrode. As illustrated in Fig. 1, the 3 mm diameter tube had to be inserted into the 5 mm NMR tube and the gold film was coated on the outside of the inner tube. Due to the restricted room in a 5 mm NMR cell, one of the electrodes (either reference or counter electrode) had to be placed inside the inner glass tube so as to effectively utilize its space. In this configuration, reference and counter electrodes were separated. Small holes were bored into the inner tube in order for the ions from the electrolyte to pass between electrodes. Both Prenzler et al. [12] and Webster [13] used this strategy (*i.e.*, coated a gold film on the outside of a tube) but used larger size NMR tubes (*e.g.*, 10 mm diameter and larger) and demonstrated satisfactory NMR results.

In the present work, two sequential coatings were performed on each glass tube to be used as the working electrode. First, the lower section of the tube was coated uniformly with a thin layer of gold. This section is to be placed in the rf region of an NMR spectrometer and requires good homogeneity. Second, the upper section of the tube was coated with relatively thicker gold in order to yield an enhanced electrical connection with the lead wire to the potentiostat. This thicker gold did not need to be uniform; rather, coating

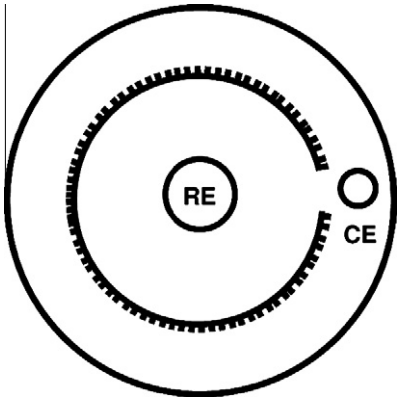

Fig. 1. Sketch showing a gold film thermally coated on the outside of a 3 mm glass tube to be used as a working electrode. The outer circle represents a 5 mm NMR tube. Holes (represented by a gap in the 3 mm tube) are bored into the inner tube to create ion paths among all three electrodes. Drawings are not to scale.

only one side of the glass tube was sufficient. An overlap area was necessary between the upper and lower regions.

A E12E4 thermal evaporator (Edwards) was applied to coat the outer surface of the 3 mm glass tubes. The gold was deposited by thermal evaporation at 1000–1100 °C in vacuum (*ca.* 3×10^{-6} Torr). To coat the lower section, the glass tube was attached horizontally to a homemade rotor that was located 12 cm above the gold source. The rotor rotated in the range of 180–200 revolutions per minute, which was faster than the speed of gold deposition. The thickness of the gold coating was monitored and controlled using a quartz crystal thickness monitor, which is standard instrumentation for vacuum deposition systems.

The portions of the tube which were not to receive gold were covered with PTFE tape. The second segment of gold started from a 5 mm overlapping section with the uniform gold film in the lower section. Stationary coating (*i.e.*, without rotation) was performed. Since this upper band of gold film was only coated on one side of the glass tube, the resultant thickness could be read directly from the thickness monitor (no compensation is necessary). The gold film applied in the upper section was five times thicker than the lower section. This extra thickness was required to reduce its resistance.

As a working electrode, the prepared gold film included a 4 cm length of a uniform film (evenly coated around the glass tube) with a 20 nm thickness and a 4.5 cm length of a film (only coated on one side of the glass tube) with 100 nm thickness. The total resistance of the gold film was typically found to be 10–20 Ω by a four point resistance measurement. The measured resistance is similar to the theoretical calculation (*i.e.*, around 10 Ω) and the slight difference might cause problems in electrochemical studies, such as an uneven current distribution over the surface of the working electrode.

2.1.2. Counter electrode and reference electrode

In a three-electrode cell, the current flows between working and counter electrodes. Effective electrochemical measurement is based on the assumption that the measured impedance comes entirely from the working electrode. This can be achieved by ensuring a very small resistance and a very large capacitance of the counter electrode. The larger the area of the counter electrode, the smaller its resistance and the bigger its capacitance. Therefore, in practice, the active size of a counter electrode should be as much as 100 times the size of the working electrode. In this work, this area ratio was hard to obtain due to the use of a large working electrode as well as a very limited cell size. Consequently, effort was put into making the counter electrode as small as possible in physical size (in order to fit inside a 5 mm NMR tube) while presenting the largest possible surface area.

To place the counter electrode outside the 3 mm glass tube, the overall electrode thickness is crucial. The gap between the 3 mm glass tube and the 5 mm NMR tube (with a wall thickness of 0.38 mm) is 0.6 mm. Therefore, a very thin curved counter electrode had to be constructed for this configuration. A platinum foil counter electrode (0.06 mm thickness) was therefore prepared by spot welding a 0.3 mm diameter platinum wire onto the narrow side (*i.e.*, 3 mm) of the platinum foil with a size of 3 mm × 40 mm. It was then manually curved according to the curvature of the 3 mm glass tube. After cleaning by submerging in warm concentrated HNO_3 (68–70%) for 20 min, the platinum counter electrode was platinized with the intention of increasing the effective surface area. In pairs, two homemade counter electrodes were immersed in a 0.05 M H_2PtCl_6 solution with lead acetate. A 30 mA current was passed between the pair of platinum electrodes and the current direction was alternated every 30 s. The platinization procedure was considered to reach completion after both electrodes turned black. They were then rinsed with water and were ready to use.

A customized 120 mm long leak-free Ag/AgCl electrode (Warner Instruments) was used as a reference electrode. This Ag/AgCl reference electrode has an outer diameter of 1 mm and could fit inside the inner 3 mm tube. The cell thus constituted of the curved platinum foil counter electrode, which is positioned outside the 3 mm glass tube, the thin film working electrode on the 3 mm tube and the reference electrode in the center of the 3 mm tube.

2.1.3. ECNMR cell assembly

The main body of the ECNMR cell is illustrated on the left of Fig. 2. Both the enlarged view and the top view of the dotted area are shown by the sketches on the right. The outer compartment (a) was a 5-mm-o.d. high precision NMR tube (Wilmad 506-1M, Pyrex) affixed to a thicker-walled 7-mm-o.d. glass tube (b). This 7-mm-o.d portion offered an improved resistance to cracking as well as a bigger working space (see Fig. 3).

A thin gold film-coated 3-mm-o.d. glass tube (d) was positioned inside the 5-mm-o.d. NMR tube to function as the working electrode. A glass rim was made towards the bottom of the 3-mm-o.d. glass tube (also referred to as the inner glass tube) for the purpose of centering. Three small holes (o) were cut in the inner glass tube to facilitate the transfer of ions. The gold film working electrode was made up of two sections. The lower section

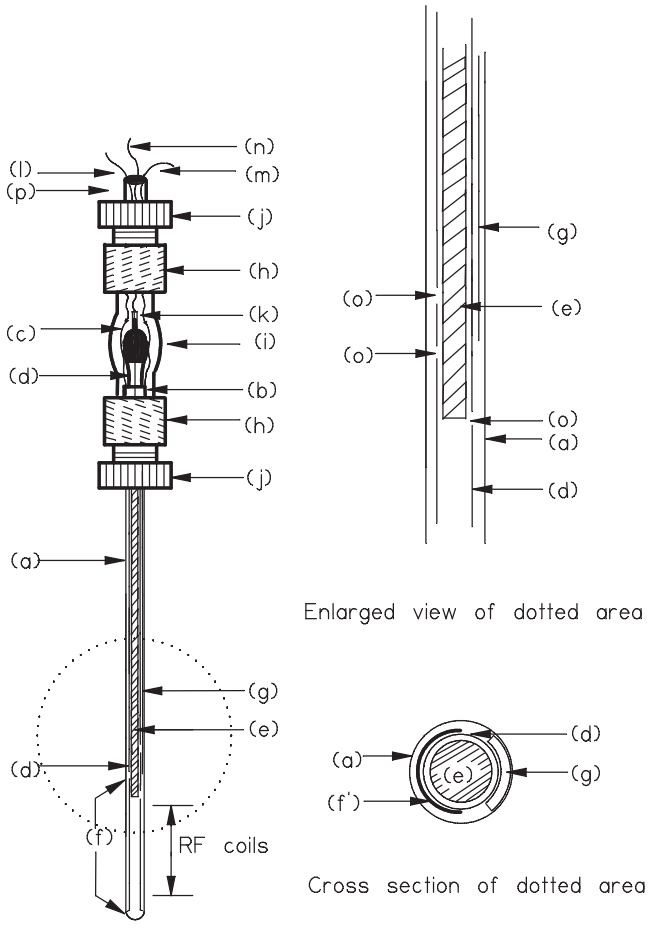

Fig. 2. Left: Side view of the ECNMR cell; Top right: Enlarged drawing of the dotted area; Bottom right: Cross section of the dotted area. (a) 5-mm-o.d. NMR tube, (b) 7-mm-o.d. glass tube, (c) working electrode copper lead, (d) 3-mm-o.d. glass tube, (e) reference electrode, (f) 20 nm uniform gold film working electrode, (f′) 100 nm gold film working electrode (on one side of the inner tube), (g) platinum counter electrode, (h) number 7 glass adapters, (i) 12-mm-o.d. glass tube, (j) 7.5-mm-PTFE bushings, (k) electric snap-in connector, (l, m and n) leading wires of three electrodes, (o) small holes in the 3-mm-o.d. glass tube, and (p) 7-mm-o.d. glass tube.

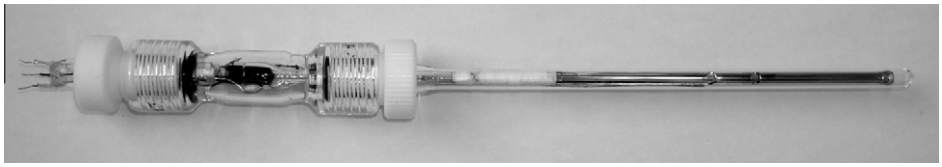

Fig. 3. Photograph of fully assembled ECNMR cell.

(f, 20 nm thick) was a uniform cylindrical gold film, which was positioned on the inner glass tube between the glass rim and the small holes. It had a length of 40 mm and was placed in the rf region of the NMR spectrometer during experiments. The second segment of the gold film (f′, 100 nm thick) was positioned on the inner glass tube above the first section with a 5 mm overlapping (between the bottom two holes) area. The thicker gold film had a length of 45 mm in total and was coated on one side of the glass tube. A piece of platinum foil was wrapped tightly at the top section of the 100 nm gold film. One end of a thin copper wire (c) was soldered to the platinum foil and the other end was connected to a copper lead (l) that linked to the potentiostat. The soldered section was covered with PTFE tape, which would be above the electrolyte solution during all experiments. A reference electrode (e) was inserted inside the 3-mm-o.d. glass tube with its tip positioned at one of the small holes (o). A curved platinum gauze/foil counter electrode (g) was positioned between the inner glass tube and the outer NMR tube.

Two identical number seven glass adapters (Ace Glass Inc., 5027-05) (h) were connected tail-to-tail with a section of a 12-mm-o.d. glass tube (i), which housed the cap-in connector (k) to the reference electrode as well as the lead wires of the other two electrodes. A pair of 7.5-mm-PTFE bushings (Ace Glass Inc., 5029-35) (j) were screwed into these two glass adapters (h) to hold all glass tubes in position. O-rings were used on the 7-mm-o.d. glass tubes (b and p) to ensure an air-tight seal. All leading wires (l, m and n) to the three electrodes were fixed to the 7-mm-o.d. glass tube (p) by epoxy.

The assembly of this ECNMR started with connecting all three electrodes to their leading wires either by a snap-in connector (k) or by a soldering technique. Then all components were transferred to a glove box. The assembly of all other sections was performed inside a glove box.

A NMR sample tube holder (also called a spinner) was homemade from Delrin (polyoxymethylene), which is commonly used in engineering plastics as a metal substitute. This material is light-weight and is capable of operating at various temperatures. The Delrin holder was constructed with the same specifications as a commercial NMR tube holder but had a longer (not wider) upper section. This lengthened section was used to house the main body of the ECNMR cell (Fig. 2 left). In this way, the ECNMR cell was entirely protected inside the Delrin holder, which could be readily fit into a commercial NMR instrument. Three holes were drilled in the Delrin cap, which was incorporated in the sample holder. Three male connectors were securely fixed inside these holes. All leading wires (l, m and n) were soldered to these male connectors from inside. On the outside, pins were snapped in for connection and then lead to a potentiostat.

2.1.4. Noise control strategies

In order to execute electrochemical and NMR experiments simultaneously, the computer-controlled potentiostat was placed on a cart and brought to the NMR facility room. As shown in Fig. 4, the potentiostat was positioned about two meters from the NMR magnet. This distance was adopted to minimize the influence on the potentiostat from the strong magnetic field. The rf shielded connecting cables to the three electrodes were two and a half meters long. Both chokes in the potentiostat and low-pass filters in the electrode leads were applied to minimize the interference between the potentiostat and the NMR spectrometer.

A flexible copper-braided shield was used to house the three rf shielded cables. The copper shield guided these cables from the

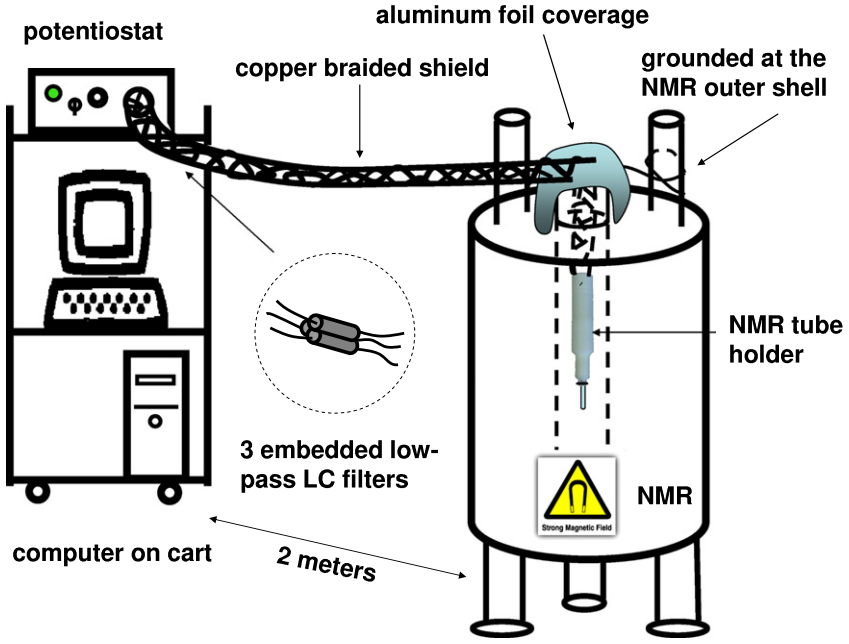

Fig. 4. Sketch of experimental setup of an *in situ* ECNMR experiment. Important noise control segments were labeled in figure.

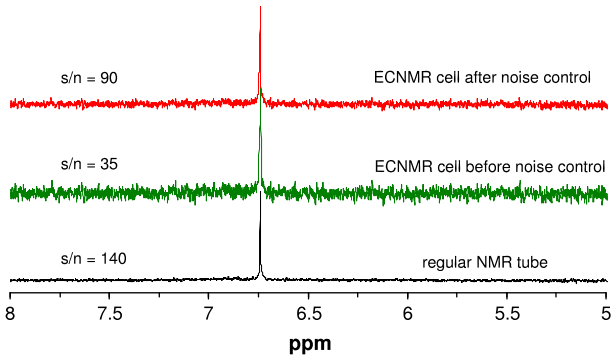

Fig. 5. NMR spectra of 5 mM benzoquinone in a HCl solution (pH 0.5). The top two spectra were acquired in the ECNMR cell with and without the noise control performance, respectively. The bottom spectrum was acquired in a regular NMR tube. The values of the signal-to-noise ratio are reported beside each spectrum.

potentiostat to the homemade sample tube holder that was placed inside the NMR bore. The outer shield was open to the potentiostat and grounded to the probe ground at the NMR outer shell. An aluminum foil was used to cover the opening of the NMR bore to further reduce the noise.

The noise control strategies greatly increased the signal-to-noise ratio of the NMR spectra. Fig. 5 compares the NMR spectra of benzoquinone with and without the noise control steps. The bottom trace shows the spectrum of benzoquinone at pH 0.5 in a 5 mm NMR tube; in the ECNMR cell the sample volume is decreased by about 36%, due to confinement between the 3 mm and 5 mm tubes. The reduction in signal-to-noise ratio from 140 to 90 is in about this ratio, indicating that the electrical noise reduction strategies were quite effective.

3. Results and discussion

3.1. Probe performance: studies of 1,4-benzoquinone

1,4-Benzoquinone was chosen to study because it is easy to work with and has been well-studied electrochemically both in aqueous [18–21] and non-aqueous [22–24] solutions. The evolution of NMR spectra with time upon the reduction to hydroquinone has also been reported [4,11,12,14]. However, no simultaneous electrochemical data along with NMR spectra on benzoquinone have been presented.

3.1.1. 1,4-Benzoquinone in an aqueous solution

The electrolysis products of benzoquinone in dilute H_2SO_4 were characterized in the ECNMR cell constructed in-house. The electrolyte was 7.7 mM 1,4-benzoquinone dissolved in 0.15 M H_2SO_4. The ECNMR cell was assembled with electrolyte inside a N_2 glove box to maintain an oxygen-free environment. Fig. 6 demonstrates the reaction for the reduction of benzoquinone. The H_2SO_4 solvent provides sufficient proton donors required for the reaction. This well-studied reaction [4,11,12,14,18–21] was selected in order to evaluate the function of the ECNMR cell. The NMR spectra of the

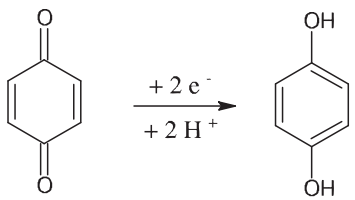

Fig. 6. Reduction of benzoquinone in an aqueous solution.

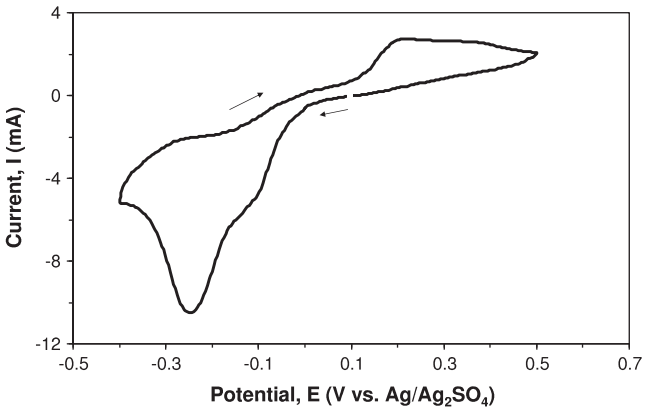

Fig. 7. Cyclic voltammogram of 7.7 mM 1,4-benzoquinone in 0.15 M H_2SO_4 at a 20 nm gold film electrode at the sweep rate of 100 mV s^{-1}. It was acquired inside a NMR probe.

four phenyl protons in benzoquinone and hydroquinone are similar. Both spectra consist of singlets, with slightly different chemical shifts. The cyclic voltammogram of benzoquinone in the NMR probe is presented in Fig. 7. To our knowledge, no documented account of a cyclic voltammogram acquired inside a NMR probe have been published. It makes Fig. 7 the first *in situ* cyclic voltammogram in this field. The starting potential was 0.1 V (corresponding to zero in current) and swept cathodic before anodic. The reduction peak was bigger than the oxidation peak. This can be explained by diffusion: after reduction, the reduced species (*i.e.*, hydroquinone) diffused away from the electrode surface and only a portion was left (or diffused back) to be reoxidized upon the reverse reaction.

Electrolysis was performed in order to generate exclusively the reduced species at the potential of −0.4 V, where reduction takes place. *In situ* ECNMR spectra were recorded simultaneously and are shown in Fig. 8. The series of NMR spectra was collected during the course of the electrochemical reactions. Before electrolysis, the phenyl protons in benzoquinone showed a singlet at 6.74 ppm (bottom spectrum in Fig. 8). After 1 min of electrolysis, a second peak appeared at 6.66 ppm, indicating the formation of hydroquinone. The spectra acquired during a 10 min time frame depicted the general trend of the evolution between the two species. The increasing peak at 6.66 ppm was due to the production of hydroquinone and the decreasing peak at 6.74 ppm was due to

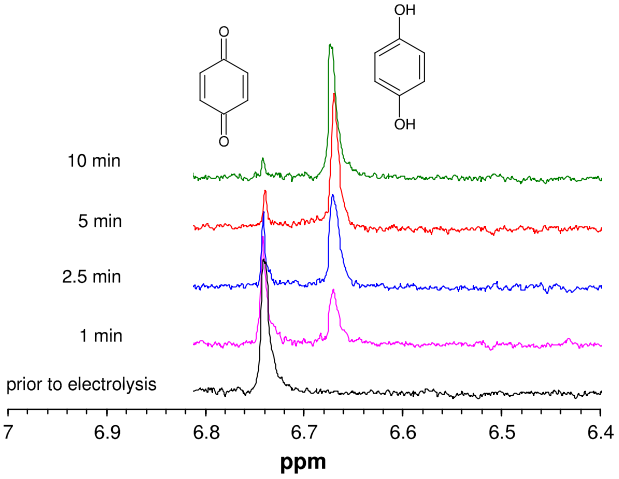

Fig. 8. *In situ* ECNMR spectra for the reduction of benzoquinone. Conditions: 7.7 mM 1,4-benzoquinone in 0.15 M D_2SO_4, $E_{applied} = -0.4$ V. All spectra were obtained in the ECNMR cell positioned inside the NMR probe. NMR spectrum of benzoquinone prior to electrolysis is also included for comparison.

the consumption of benzoquinone. An NMR spectrum of hydroquinone in D_2SO_4 was also performed (not shown) and confirmed that the lower frequency signal was indeed caused by the phenyl protons in hydroquinone. The results demonstrated that the *in situ* ECNMR cell could be used in a 5 mm high-resolution NMR probe in aqueous solution.

Upon further electrolysis, there was no change observed in the peak intensity of both phenyl protons, suggesting that not all benzoquinone was reduced to hydroquinone even with an extended reduction period. As shown in Fig. 2, electrolyte was present both inside and outside of the 3 mm glass tube. Benzoquinone that was inside the 3 mm glass tube could only diffuse through the small holes in order to contact the gold film working electrode. Thus it was difficult for the electrolyte to be reacted to completion. However, this incomplete reaction was not a concern. As long as a certain amount of product would be produced and spectrally resolved from the starting material, the ECNMR cell would have completed its role in detecting and characterizing the products/reactions under study.

In light of these results, the ECNMR cell constructed in-house is a true electrochemical NMR device and is able to perform *in situ* electrochemical studies. Simultaneous spectroscopic characterization was carried out successfully in an aqueous solution using a three-electrode cell.

3.1.2. 1,4-Benzoquinone in non-aqueous solution

The cell performance in an aprotic non-aqueous solvent was also tested by the reduction of benzoquinone. Unlike in aqueous solutions, there are no protons available to form hydroquinone and therefore the quinone anion is the product. The reaction is shown below in Fig. 9. There are two major differences upon the change of solvent. The first difference could be the type of the reference electrode. When water-based HCl or H_2SO_4 was used, the reference electrode could be Ag/AgCl or Ag/$AgSO_4$. These electrodes could easily be made in-house by coating a thin layer of AgCl or $AgSO_4$ on the outside of a silver wire. As a result, the overall size of the reference electrode was similar to the size of a single wire and could fit conveniently inside the ECNMR cell. However, in the case of a non-aqueous solvent, the filling solution, which contains the proper ions for the reference electrode, has to be separated from the electrolyte. This compartment would add extra width and would be impractical for use in the 5 mm ECNMR cell. Instead, a customized leak-free Ag/AgCl electrode (Warner Instruments) with an outer diameter of 1 mm, compatible with aprotic solvents, was used.

The second challenge is the supporting electrolyte. In the solution of HCl or H_2SO_4 at low pH values, such as pH 0.5, the use of an additional supporting electrolyte was unnecessary. The acidic solvent itself provided enough protons in order to maintain a high ionic strength of solution, which in turn had a relatively low solution resistance. However, in the case of an organic solvent, a supporting electrolyte is usually needed in order to ensure a high electrolyte conductivity. The choice of an adequate supporting electrolyte in the ECNMR cell is critical. In addition to the appropriate solubility and potential window under conventional conditions, the NMR signals of the chosen supporting electrolyte need to be away from the

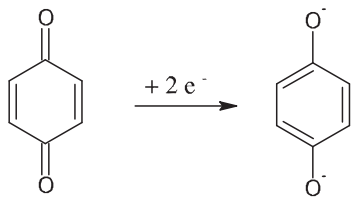

Fig. 9. Reduction of benzoquinone in a non-aqueous aprotic solution.

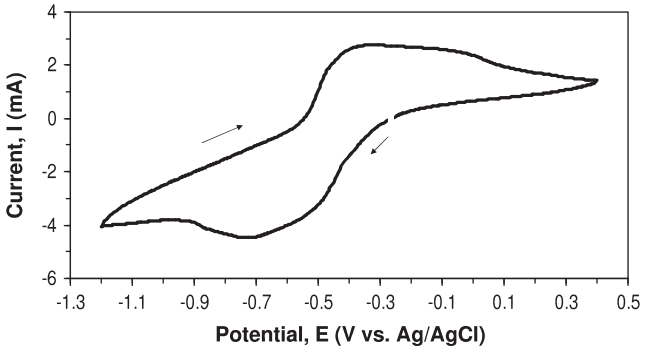

Fig. 10. Cyclic voltammogram of 7.7 mM 1,4-benzoquinone in 10 mM Bu_4NPF_6 and acetonitrile at a 20 nm gold film electrode at the sweep rate of 100 mV s^{-1}. It was acquired inside a NMR probe.

electroactive species under study. Moreover, the concentration of the supporting electrolyte should not be too high compared to the analyte, otherwise very weak NMR signals would be detected.

The same analyte, benzoquinone, was chosen for the non-aqueous study. Benzoquinone (7.7 mM) and Bu_4NPF_6 (10 mM) were dissolved in acetonitrile in a N_2 glove box. The ECNMR cell was assembled in this glove box to maintain an air-free environment. Fig. 10 shows the reduction and re-oxidation of benzoquinone in acetonitrile at the sweep rate of 100 mV s^{-1}. Fig. 10 was acquired in the ECNMR cell inside a NMR probe. Similarly to the cyclic voltammogram in the aqueous solution, it started at −0.3 V, where no current was present. The cyclic voltammetry was performed toward reduction before oxidation and two distinct peaks were observed. The difference in peak potential between aqueous and non-aqueous solutions (Fig. 7 *vs.* Fig. 10) was believed to be caused by a solvent effect.

Compared to the reactions in an aqueous solution, the redox behavior of benzoquinone/hydroquinone system in an aprotic medium is generally considered to be more complicated [25]. Both one pair [25,26,22,23] and two pairs [26,23,24] of redox peaks have been observed for the cyclic voltammetric analysis of benzoquinone in non-aqueous solutions. A variety of factors could contribute to the changes in redox peaks, such as the surface conditions of the working electrode [25], the applied sweep rate [26] and the use of different supporting electrolytes [27]. Under the conditions used in this study, one pair of redox peaks was observed in the cyclic voltammogram. The cathodic and anodic potentials were −0.7 V and −0.4 V, respectively.

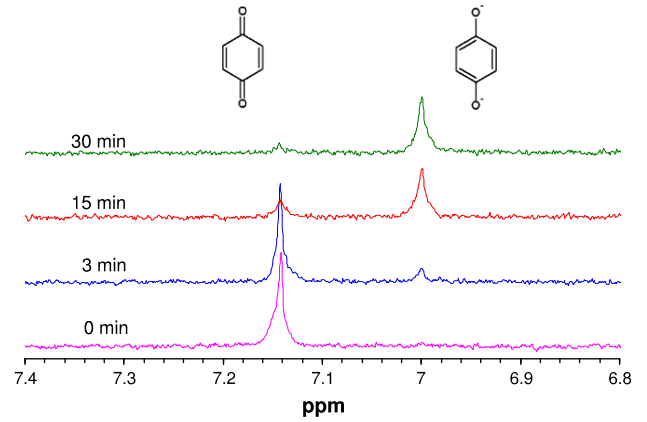

Fig. 11. *In situ* monitoring of the reduction of benzoquinone by NMR spectroscopy. Conditions: 7.7 mM 1,4-benzoquinone in 10 mM Bu_4NPF_6 and acetonitrile, $E_{applied}$ = −1.0 V. All spectra were obtained in the ECNMR cell and the time intervals are labeled in figure. Spectrum of benzoquinone prior to electrolysis (*i.e.*, 0 min of electrolysis) is included for comparison.

Electrolysis was performed at −1.0 V for the reduction of benzoquinone and a series of NMR spectra (Fig. 11) was recorded simultaneously. The phenyl protons of benzoquinone showed a singlet at 7.14 ppm before electrolysis (*i.e.*, 0 min reaction time). After 3 min of reduction, the appearance of a second peak was observed at 7.0 ppm, suggesting the formation of a quinone anion. During a 30 min period, the peak at 7.0 ppm gradually increased and the peak at 7.14 gradually decreased. This feature indicated the formation of the quinone anion from benzoquinone.

Both electrochemical and NMR results demonstrated the successful application of the ECNMR cell in non-aqueous solutions. These are, for the first time, simultaneous *in situ* ECNMR spectra accomplished inside a 5 mm high-resolution NMR probe in a non-aqueous solvent.

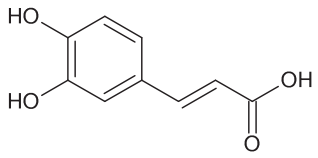

Fig. 12. Chemical structure of caffeic acid.

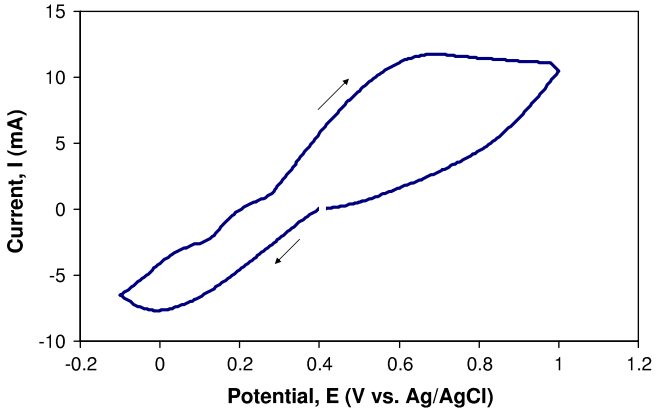

Fig. 13. Cyclic voltammogram of 5 mM caffeic acid and 40 mM Bu_4NPF_6 in (50/50) aqueous (pD 2)/acetonitrile (deuterated) at a gold film working electrode. Sweep rate $v = 100$ mV s^{-1}. It was acquired inside a NMR probe.

3.2. Application 1: Oxidation of caffeic acid

Caffeic acid, 3,4-dihydroxycinnamic acid, is a naturally occurring organic compound. This yellow solid contains both phenolic and acrylic functional groups, as shown in Fig. 12. Caffeic acid is one of many phenolics considered to have antioxidant behavior and act against immunoregulation diseases [28–32]. Besides its medical properties, the oxidation of caffeic acid has been believed to be responsible for the browning effect in food and beverages, especially in the production of wines [33–35]. Browning is the most serious phenomenon of degradation suffered by white wines after bottling and could cause a loss in nutritional and aesthetic values. However, the oxidation mechanism of caffeic acid is not well understood and therefore greatly limits its application.

There are three methods for the oxidation of caffeic acid, namely, enzymatic oxidation, chemical oxidation and electrochemical oxidation. The electrochemical oxidation method is closer to nature than chemical oxidation and it has been assumed to share similar mechanisms in biological systems [36].

A wide range of solvents has been used for the investigation of caffeic acid, including aqueous solutions [37,28], organic solvents [30], or a mixture of the two [34,38–41]. The solubility of caffeic acid in water is low at room temperature and increases significantly at about 50 °C. It has therefore been suggested to dissolve caffeic acid at temperatures between 50 °C and 95 °C when preparing aqueous solutions [42]. In this study, acetonitrile was used as a co-solvent in order to maintain all experiments at ambient temperature. The mixture of water and acetonitrile was found particularly

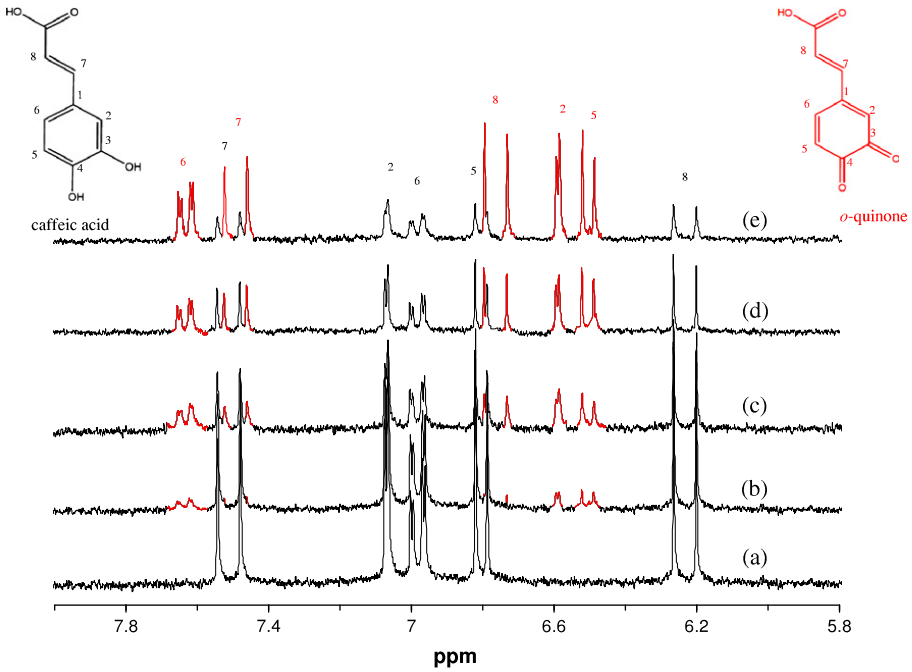

Fig. 14. *In situ* monitoring of the oxidation of caffeic acid by NMR spectroscopy. Conditions: 5 mM caffeic acid and 40 mM Bu_4NPF_6 in a (50/50) aqueous (deuterated, pD 2)/acetonitrile (deuterated) solution, $E_{applied} = 1$ V. All spectra were obtained in the ECNMR cell at different time intervals: (a) prior to electrolysis; (b) 10 min; (c) 20 min; (d) 40 min and (e) 70 min after reaction started. All H peaks are assigned and labeled in the responding structures.

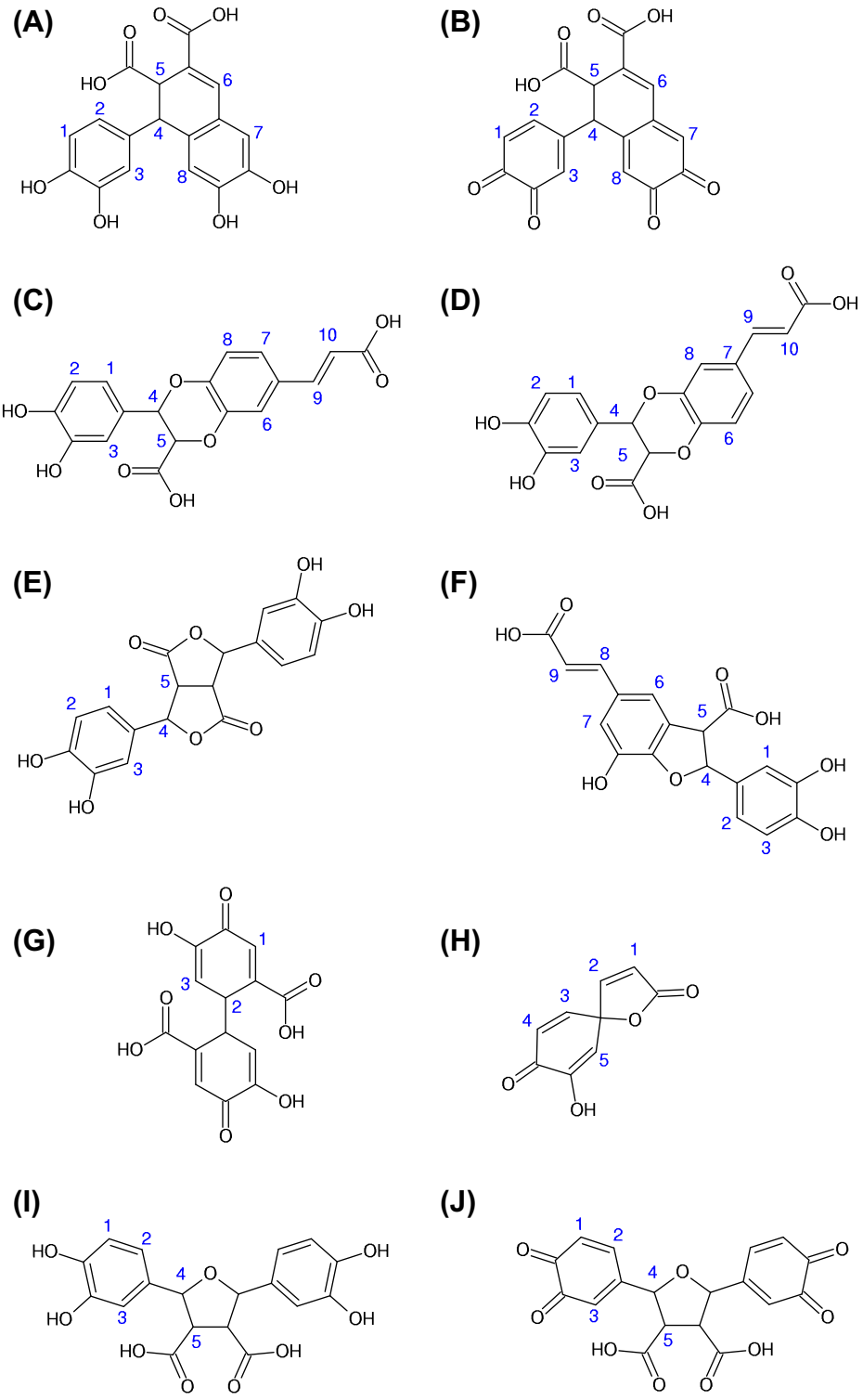

Fig. 15. List of predicted oxidation products of caffeic acid. Protons are labeled except –OH and –COOH groups. References: (A) [39], (B) [39], (C) [39,46], (D) [46], (E) [39,37], (F) [39], (G) [45,35], (H) [30], (I) [41,38,33] and (J) [41,38].

suitable to mimic biological systems due to its low polar nature and partially aqueous content [43,44].

Electrochemical studies that have contributed to understanding the behavior of caffeic acid were mostly carried out on different types of carbon electrodes [34,37,38,28,39,31,32]. In this work, a gold electrode was mainly used. Gold has been regarded as an ideal solid electrode to study the fundamentals of aromatic compounds, which do not completely oxidize (*e.g.*, form CO_2) on its surface [40].

The objectives of the present work were to study the electrochemical behavior of caffeic acid in wine-like solutions. The formation of dimers/trimers upon oxidation of caffeic acid have been reported [45,46,33,37–39,41,30,35] and the oxidation products have been characterized in the ECNMR cell.

For the *in situ* ECNMR study, the concentration of caffeic acid used was 5 mM in order to obtain better signal-to-noise ratios for the NMR spectra. Deuterated solvents were used in the

Table 1
Summary of the predicted ^{1}H NMR chemical shifts of compounds mentioned in the literature as possible oxidation products of caffeic acid (see Fig. 15).

Compound	H-1	H-2	H-3	H-4	H-5	H-6	H-7	H-8	H-9	H-10
(A)	6.61	6.61	6.63	4.77	4.10	7.19	6.72	6.48	–	–
(B)	6.63	7.40	6.63	3.57	3.55	7.39	7.01	6.88	–	–
(C)	6.65	6.60	6.58	5.80	5.07	6.99	7.17	6.98	7.78	6.51
(D)	6.64	6.56	6.56	5.80	5.07	6.76	6.99	6.97	7.75	6.50
(E)	6.60	6.60	6.67	6.92	3.55	–	–	–	–	–
(F)	6.68	6.67	6.61	5.70	4.53	7.21	6.76	7.62	6.61	–
(G)	7.27	2.92	6.85	–	–	–	–	–	–	–
(H)	6.28	7.63	7.80	6.51	5.60	–	–	–	–	–
(I)	6.60	6.70	6.64	5.54	3.33	–	–	–	–	–
(J)	6.71	7.54	6.83	4.94	2.98	–	–	–	–	–

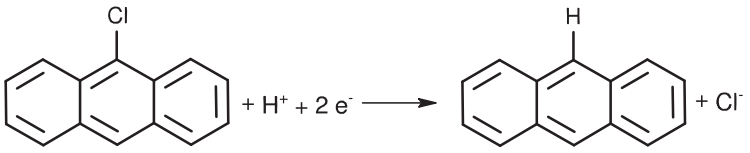

Fig. 16. Reduction of 9-chloroanthracene to anthracene.

$$ArCl + 1\,e^- \rightleftharpoons ArCl^{\bullet -} \quad (1)$$

$$ArCl^{\bullet -} \longrightarrow Ar^{\bullet} + Cl^- \quad (2)$$

$$Ar^{\bullet} + 1\,e^- \rightleftharpoons Ar^- \quad (3)$$

$$Ar^{\bullet} + ArCl^{\bullet -} \longrightarrow Ar^- + ArCl \quad (4)$$

$$Ar^- + H_2O \longrightarrow ArH + OH^- \quad (5a)$$

$$Ar^- + R'CH_2N^+R_3 \longrightarrow ArH + R'C^-HN^+R_3 \quad (5b)$$

$$Ar^- + SH \longrightarrow ArH + S^- \quad (6)$$

$$Ar^{\bullet} + SH \longrightarrow ArH + S^{\bullet} \quad (7)$$

$$S^{\bullet} + 1\,e^- \rightleftharpoons S^- \quad (8)$$

$$S^{\bullet} + ArCl^{\bullet -} \rightleftharpoons S^- + ArCl \quad (9)$$

$$S^- + H^+ \longrightarrow SH \quad (10)$$

Fig. 17. Proposed mechanism for the reduction of 9-chloroanthracene.

non-buffered solution at pD 2. A cyclic voltammogram (Fig. 13) was obtained to check the performance of the prepared solution. A relatively narrow potential window was used in order to focus on the oxidation peak. Background subtraction was performed to eliminate any effect of the gold electrode. Within the NMR probe, the CV exhibited the expected oxidation peak at 0.7 V, which was close in value to that acquired outside the NMR probe (not shown).

NMR spectra were collected simultaneously during the course of the electrochemical reactions with the applied potential of 1.0 V. NMR data both prior to reactions and at different intervals into oxidation are plotted in Fig. 14. During oxidation, the proton signals 6 and 8 were deshielded (0.65 ppm and 0.53 ppm, respectively) and the proton signals 2 and 5 were shielded (0.48 ppm and 0.31 ppm, respectively) with regard to the protons in caffeic acid. The effect on proton 7 was negligible. The time evolution of NMR spectra clearly showed the formation of *o*-quinone, whose signals were observed to be stable over 1 h, suggesting the relative stability of the *o*-quinone product under conditions applied in this research.

Structures of other possible oxidized products proposed in published papers are listed in Fig. 15. All protons were labeled except those in hydroxyl and carboxyl groups, whose chemical shift is difficult to predict due to the proton exchange. MestReNova software was used to calculate the values of chemical shift, which are displayed in Fig. 1. Upon comparison, no signals of these oxidized products were evident from the NMR spectra in Fig. 14. Therefore, only *o*-quinone was formed under the conditions applied. There are no indications of dimers or trimers from the NMR analysis (see Table 1)

3.3. Application 2: Reduction of 9-chloroanthracene

The electrochemical reduction of halogenated organic compounds has been studied for many years and remains a subject of interest for both mechanistic and synthetic issues [47–50]. The cleavage of a carbon–halogen bond upon reduction has been widely explored to characterize and understand the processes involved.

The carbon–halogen bond cleavage occurs differently in alkyl and aryl halides. The reduction of an alkyl halide brings about a simultaneous bond dissociation. However, in the case of an aryl halide, electron transfer takes place first, followed by bond cleavage [51]. 9-Chloroanthracene belongs to the latter category and therefore its reduction follows a sequential route. The reduction of 9-chloroanthracene to anthracene is shown in Fig. 16.

The electrochemical reduction of 9-chloroanthracene has been studied by different research groups [49–53]. Its cyclic voltammogram at an inert electrode (glassy carbon or gold) in acetonitrile has been reported. Upon reduction, it exhibited a chemically irreversible first reduction peak followed by another reductive peak (or peaks). The first irreversible peak was attributed to the cleavage of the carbon–chlorine bond; however, the explanation of its second peak was controversial. While some papers [51,52] assigned the second reduction peak to the formation of an aryl anion from its radical precursor due to a cleavage reduction, others [49,50,53] have stated that it was a further reduction of the previously formed anthracene.

This disagreement is at the root of the controversy concerning the reduction mechanism of 9-chloroanthracene. In the former

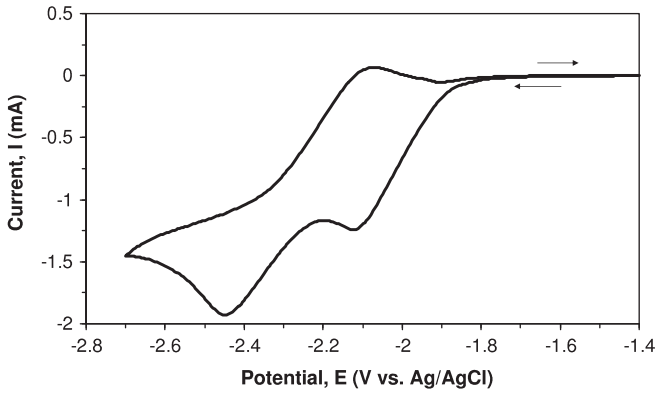

Fig. 18. Cyclic voltammogram of 5 mM 9-chloroanthracene in 10 mM Bu_4NPF_6 and acetonitrile at a gold wire electrode at the sweep rate of 100 mV s^{-1}.

case, the cleavage of the carbon–chlorine bond is thought to be in a step wise manner, which includes both the production of a radical (*i.e.*, first peak) and the production of the aryl anion (*i.e.*, second peak). On the other hand, the latter view hypothesized that the formation of an aryl anion from 9-chloroanthracene occurs in a single step, which contributed to the first irreversible reduction peak in the cyclic voltammogram. One of the proposed mechanisms [13,51,54] is shown in Fig. 17. The overall electrochemical reaction of 9-chloroanthracene (ArCl) in non-aqueous media involves two electrons, which are transferred in (1) and (3), respectively. The reduction starts with a one-electron heterogeneous transfer at the electrode surface (1) and forms a radical anion $ArCl^{\cdot -}$, which decomposes to yield the anthracene radical ($Ar^{\cdot}$) and the chloride anion (Cl^-) in step (2). The neutral radical $Ar^{\cdot}$ formed from the carbon–chlorine bond cleavage is, in general, more easily reducible (*i.e.*, has a more positive reduction potential) than the parent ArCl molecule and can be further reduced to anthracene anion (Ar^-). The formation of Ar^- can occur either at the electrode surface (3) or by homogeneous electron transfer with the initially generated radical anion $ArCl^{\cdot -}$ (4). Reactions (1)–(3) constitute an Electrochemical–Chemical–Electrochemical (ECE) mechanism and reactions (1), (2) and (4) are known as a DISP1 (first disproportionation) pathway [55]. The anthracene anion is a strong base and will be readily protonated by any proton donor available in solution, such as residual water (5a) or supporting electrolyte (5b). Acidic impurities from the solvent itself (SH) is also a possible route, even though it is less likely, to form the final product anthracene (ArH) (6). Alternatively, anthracene radical formed from reaction (2) can attract a hydrogen from the solvent through HAT (hydrogen atom transfer) to form ArH (7). The solvent radical $S^{\cdot}$ formed in this way can be reduced either at the electrode surface (8) or in solution (9). Solvent anions (S^-) can be protonated when protons are available (10). In this mechanism, reactions (1)–(7) contribute to the formation of anthracene and will be considered below. The work described in this section has therefore been designed to study the reduction mechanism of 9-chloroanthracene.

The cyclic voltammogram of the reduction of 9-chloroanthracene was obtained at a gold wire working electrode with 10 mM Bu_4NPF_6 at the sweep rate of 100 mV s^{-1}. The acquired CV is present in Fig. 18, which shows two successive reduction peaks followed by one oxidation peak on the back sweep. The appearance of this cyclic voltammogram is similar to what has been reported by other researchers [49–53]. The concentration of Bu_4NPF_6 was chosen to be 10 mM in order to minimize its signal strength in NMR analysis.

ECNMR was performed to study the reactions involved with these cyclic voltammetric peaks (*cf.* Fig. 18), especially the controversial statements about the second cathodic peak at −2.45 V. The reduction of 9-chloroanthracene was investigated by means of controlled potential electrolysis and monitored simultaneously by ECNMR inside an NMR probe. Two potentials were chosen to cause the reduction to proceed to different reaction stages. At −2.3 V, only the first reduction peak was completed; while at −2.7 V, both reduction peaks would have occurred. These two potentials were selected at higher potentials (*i.e.*, more cathodic) than those shown in Fig. 18. This was done in order to compensate any over-potential caused by the gold film electrode.

Both values of cathodic potentials (−2.3 V and −2.7 V) were applied for electrolysis. The NMR spectra in Fig. 19 were recorded *in situ* during the electrochemical reduction of 9-chloroanthracene at −2.3 V . The results acquired at −2.7 V (not shown) are exactly the same during the time frame of over 1 h. The middle section (four spectra in series) of Fig. 19 shows the evolutionary changes in NMR spectra upon reduction. The time interval between each

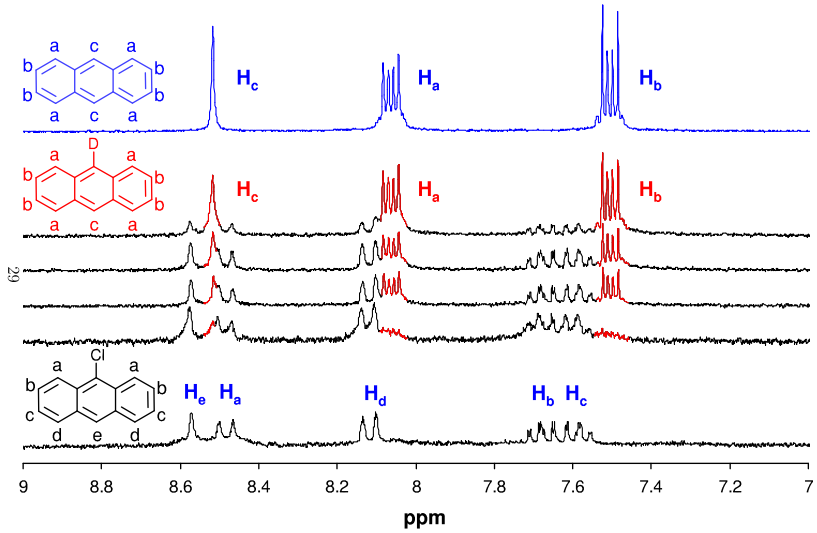

Fig. 19. Bottom: NMR spectrum of 9-chloroanthracene; Middle: *In situ* monitoring of the reduction of 9-chloroanthracene by the NMR spectroscopy. Conditions: 5 mM 9-chloroanthracene and 10 mM Bu_4NPF_6 in CD_3CN. All four spectra were obtained in the ECNMR cell at different time intervals. H peaks have been assigned and labeled in the responding structures; Top: NMR spectrum of anthracene.

spectrum was between 10 and 15 min for each potential applied. The bottom spectrum was taken before electrolysis and the top spectrum was pure anthracene in a regular NMR tube. Protons are assigned and labeled in the figure. It is apparent that anthracene was formed upon the reduction of 9-chloroanthracene.

An extended time (up to 3 h) at the potential of −2.7 V was held for electrolysis but anthracene was still the only product detected. As the potential of −2.7 V is more negative than the reduction peak at −2.45 V in Fig. 18, the second reduction peak should not be due to the reduction of anthracene. Otherwise, new products would have been produced and detected. This observation eliminated the possibility for the reduction of anthracene during the cyclic voltammetry under study. Therefore, it is more likely that the peak pair at −2.45 V and −2.1 V was due to the forming and deforming of the anthracene anion (reaction (3)) [51,52]. The mechanism listed in the introduction section agreed with this finding and will be used as guidance for the investigation of the reduction of 9-chloroanthracene.

At −2.3 V, only the first reduction peak was completed and the reaction that occurred corresponded to (1) and (2) in the proposed mechanism [13,51,54]. The only route to form anthracene without Ar^- was reaction (7). Therefore, the presence of anthracene at −2.3 V indicated that reaction (7) had to take place. At −2.7 V, the proposed reaction mechanism took place up to reaction (3). The resultant product, anthracene, could come from (5), (6) or (7). The integration of H_c in Fig. 19 of the final product is about half the size of the H_c in anthracene, suggesting that protons at H_c position constituted around 50% deuterated form. This is a good indication that reaction (5) was not a major route. Route (6) is possible but could not be identified by the ECNMR method.

An extensive amount of water was added to force route (5a) to take place. Experimentally, 5 mM 9-chloroanthracene and 10 mM Bu_4NPF_6 were dissolved in a (50/50) water/acetonitrile solution and the previous ECNMR experiment was repeated. Again, very similar NMR spectra were detected upon the reduction at −2.7 V. The integrated H_c signal stayed the same, indicating that route (5a) has not likely occurred.

In this section, ECNMR data have been used to investigate the mechanism routes from (5) to (7), and only (7) was proved to take place under the conditions studied. There was no evidence for the reduction of anthracene in the acquired NMR spectra, nevertheless, it could occur. If the second reduction peak was (partially) due to the reduction of anthracene to its radical anion form ($ArH^{\cdot -}$), then reaction $ArH^{\cdot -} + ArCl \rightarrow ArCl^{\cdot -} + ArH$ must have occurred. In this study, it is reasonable to associate the second reduction peak with route (3). According to the proposed mechanism, Fig. 18 was reconciled and can be explained as follows. The first irreversible peak at −2.1 V was due to the reduction of 9-chloroanthracene to its radical anion form, which had a certain lifetime and was able to diffuse away from the electrode [56]. This diffusion is very important as it efficiently avoided the direct reduction of the relatively easily reducible radical $Ar^{\cdot}$ formed in step (2). Therefore, even though $Ar^{\cdot}$ is thought to more easily reduced [13,50], two successive reduction peaks were observed. The second reduction peak and the subsequent oxidation peak forms a reversible peak pair because of reaction (3).

4. Conclusion

A 5-mm-o.d. three-electrode ECNMR cell was designed and constructed. This homemade ECNMR cell was designed to fit any commercial NMR instrument with a 5 mm bore. In this work, a 250 MHz shared service NMR instrument was used. The details of all three electrodes were presented and the assembly of the cell was described in detail. The cooperation between the potentiostat and the NMR instrument was depicted and different approaches were applied to minimize the noise transmitted in both directions. These noise control methods were shown to be effective in cutting down background noise in the acquired NMR spectra.

In situ ECNMR studies were performed using the ECNMR cell inside a 5 mm QNP probe (Bruker 250 MHz NMR). The reduction of benzoquinone was used to test the performance of the ECNMR cell both in aqueous and non-aqueous solvents. The results were promising and proved the feasibility of the use of the ECNMR cell in both solvents. In the case of a non-aqueous solvent, it was the first time that simultaneous *in situ* ECNMR spectra were accomplished in a 5 mm high-resolution NMR probe.

In situ ECNMR work showed the formation of *o*-quinone upon oxidation. This oxidized product was stable during the course of reaction and no dimers or trimers were detected under the conditions applied. Reduction of 9-chloroanthracene in acetonitrile was investigated and the mechanism was studied. It has been confirmed by ECNMR that the second reduction peak in its cyclic voltammogram was not the reduction of anthracene. Rather, it was mostly likely to be the formation of Ar^- from $Ar^{\cdot}$. ECNMR work also confirmed the occurrence of route (7) in the proposed mechanism. Reaction (5) is not a major route and reaction (6) could take place but could not be confirmed under the present study.

Acknowledgments

We thank Professor Louis Ramaley, Dalhousie University, and Professor Richard Webster, Nanyang Technological University for advice and discussions throughout this project; the NMR-3 center at Dalhousie University for instrumental support; and Brian Millier, Jürgen Müller, Andy George, Richard Conrad, and Mike Boutilier, Dalhousie University, for extensive technical support. This work was financially supported by the National Science and Engineering Research Council of Canada.

References

[1] J.A. Richards, D.H. Evans, Flow cell for electrolysis within the probe of a nuclear magnetic resonance spectrometer, Anal. Chem. 47 (1975) 964–966.
[2] K. Albert, E. Dreher, H. Straub, A. Rieker, Monitoring electrochemical reactions by ^{13}C NMR spectroscopy, Magn. Reson. Chem. 25 (1987) 919–922.
[3] V.G. Mairanovskii, L.Y. Yuzefovich, T.M. Filippova, Electrochemical generation of radicals in the cavity of a high-resolution nuclear magnetic resonance spectrometer. Kinetics of electron transfer in the quinone–quinone radical-anion system, Russ. J. Phys. Chem. 51 (1977) 1058–1059.
[4] V.G. Mairanovskii, L.Y. Yuzefovich, T.M. Filippova, NMR-electrolysis combined method (NMREL) basic principles and some applications, J. Magn. Reson. 54 (1983) 19–35.
[5] M.E. Sandifer, M. Zhao, S. Kim, D.A. Scherson, In situ nuclear magnetic resonance determination of paramagnetic susceptibilities of electrogenerated species, Anal. Chem. 65 (1993) 2093–2095.
[6] P.J. Slezak, A. Wieckowski, Electrode potential dependent NMR spectra of surface ^{13}CO on polycrystalline platinum, J. Electroanal. Chem. 339 (1992) 401–410.
[7] J.W. Rathke, R.J. Klinger, R.E. Gerald II, K.W. Kramarz, K. Woelk, Toroids in NMR spectroscopy, Prog. NMR Spectrosc. 30 (1997) 209–253.
[8] J. Wu, J.B. Day, K. Franaszczuk, B. Montez, E. Oldfield, A. Wieckowski, P.-A. Vuissoz, J.-P. Ansermet, Recent progress in surface NMR-electrochemistry, J. Chem. Soc. Faraday Trans. 93 (1997) 1017–1026.
[9] J.C. Slater, Microwave electronics, Rev. Mod. Phys. 18 (1946) 441–512.
[10] N. Bloembergen, On the magnetic resonance absorption in conductors, J. Appl. Phys. 23 (1952) 1383–1389.
[11] D.W. Mincey, M.J. Popovich, P.J. Faustino, M.M. Hurst, J.A. Caruso, Monitoring of electrochemical reactions by nuclear magnetic resonance spectroscopy, Anal. Chem. 62 (1990) 1197–1200.
[12] P.D. Prenzler, R. Bramley, S.R. Downing, G.A. Heath, High-field NMR spectroelectrochemistry of spinning solutions: simultaneous in situ detection of electrogenerated species in a standard probe under potentiostatic control, Electrochem. Commun. 2 (2000) 516–521.
[13] R.D. Webster, In situ electrochemical-NMR spectroscopy. Reduction of aromatic halides, Anal. Chem. 76 (2004) 1603–1610.
[14] S. Klod, F. Ziegs, L. Dunsch, In situ NMR spectroelectrochemistry of higher sensitivity by large scale electrodes, Anal. Chem. 81 (2009) 10262–10267.
[15] J.B. McGee, US Pat. 4,315,970, Patented, 1982.
[16] J.J. Ponjee, J.W.A. Nelissen, C.J.A. Verwijlen, Eur. Pat. 111,957, Patented, 1984.

[17] C.A. Goss, D.H. Charych, M. Majda, Application of (3-mercaptopropyl) trimethoxysilane as a molecular adhesive in the fabrication of vapor-deposited gold electrodes on glass substrates, Anal. Chem. 63 (1991) 85–88.
[18] S.I. Bailey, I.M. Ritchie, A cyclic voltammetric study of the aqueous electrochemistry of some quinones, Electrochim. Acta 30 (1985) 3–12.
[19] A. Bott, The study of multiple electron transfer reactions by cyclic voltammetry, Curr. Sep. Drug Dev. 16 (1997) 61–66.
[20] Y. Tang, Y. Wu, Z. Wang, Spectroelectrochemistry for electroreduction of p-benzoquinone in unbuffered aqueous solution, J. Electrochem. Soc. 148 (2001) E133–E138.
[21] M. Quan, D. Sanchez, M.F. Wasylkiw, D.K. Smith, Voltammetry of quinones in unbuffered aqueous solution: reassessing the roles of proton transfer and hydrogen bonding in the aqueous electrochemistry of quinones, J. Am. Chem. Soc. 129 (2007) 12847–12856.
[22] T.W. Rosanske, D.H. Evans, Rate constant for the electrode reactions of some quinones in aprotic media at platinum, gold and mercury electrodes, J. Electroanal. Chem. 72 (1976) 277–285.
[23] V.J. Koshy, V. Swayambunathan, N. Periasamy, A reversible redox couple in quinone–hydroquinone system in nonaqueous medium, J. Electrochem. Soc. 127 (1980) 2761–2763.
[24] Y.O. Kim, Y.M. Jung, S.B. Kim, S.M. Park, Two-dimensional correlation analysis of spectroelectrochemical data for p-benzoquinone reduction in acetonitrile, Anal. Chem. 76 (2004) 5236–5240.
[25] V.D. Parker, The hydroquinone–quinone redox behaviour in acetonitrile, Chem. Commun. 13 (1969) 716–717.
[26] B.R. Eggins, Interpretation of electrochemical reduction and oxidation waves of quinone–hydroquinone system in acetonitrile, Chem. Commun. 21 (1969) 1267–1269.
[27] R.M. Scribner, Some new sulfonyl- and trifluoromethylthio-p-benzoquinones. their reactions, polarographic reduction potentials, and acid strengths, J. Org. Chem. 31 (1966) 3671–3682.
[28] C. Giacomelli, K. Ckless, D. Galato, F.S. Miranda, A. Spinelli, Electrochemistry of caffeic acid aqueous solutions with pH 2.0 to 8.5, J. Braz. Chem. Soc. 13 (2002) 332–338.
[29] H. Hotta, M. Ueda, S. Nagano, Y. Tsujino, J. Koyama, T. Osakai, Mechanistic study of the oxidation of caffeic acid by digital simulation of cyclic voltammograms, Anal. Biochem. 303 (2002) 66–72.
[30] R. Petrucci, P. Astolfi, L. Greci, O. Firuzi, L. Saso, G. Marrosu, A spectroelectrochemical and chemical study on oxidation of hydroxycinnamic acids in aprotic medium, Electrochim. Acta 52 (2007) 2461–2470.
[31] A.B. Moghaddam, M.R. Ganjali, R. Dinarvand, P. Norouzi, A.A. Saboury, A.A. Moosavi-Movahedi, Electrochemical behavior of caffeic acid at single-walled carbon nanotube: graphite-based electrode, Biophys. Chem. 128 (2007) 30–37.
[32] L.F. Silva, N. Stradiotto, H.P. Oliveira, Determination of caffeic acid in red wine by voltammetric method, Electroanalysis 20 (2008) 1252–1258.
[33] H. Fulcrand, A. Cheminat, R. Brouillard, V. Cheynier, Characterization of compounds obtained by chemical oxidation of caffeic acid in acidic conditions, Phytochemistry 35 (1994) 499–505.
[34] P. Hapiot, A. Neudeck, J. Pinson, H. Fulcrand, P. Neta, C. Rolando, Oxidation of caffeic acid and related hydroxycinnamic acids, J. Electroanal. chem. 405 (1996) 169–176.
[35] H. Li, A. Guo, H. Wang, Mechanisms of oxidative browning of wine, Food Chem. 108 (2008) 1–13.
[36] S. Suzen, B.T. Dermircigil, S.A. Ozkan, Electroanalytical evaluation and determination of 5-(3-indolyl)-2-thiohydantion derivatives by voltammetric studies: possible relevance to in vitro metabolism, New J. Chem. 6 (2003) 1007–1011.
[37] H. Tazaki, D. Taguchi, T. Hayashida, K. Nabeta, Stable isotope-labeling studies on the oxidative coupling of caffeic acid via o-quinine, Biosci. Biotechnol. Biochem. 65 (2001) 2613–2621.
[38] H. Hotta, S. Nagano, M. Ueda, Y. Tsujino, J. Koyama, T. Osakai, Higher radical scavenging activities of polyphenolic antioxidant can be ascribed to chemical reactions following their oxidation, Biochem. Biophys. Acta 1572 (2002) 123–132.
[39] R. Arakawa, M. Yamaguchi, H. Hotta, T. Osakai, T. Kimoto, Product analysis of caffeic acid oxidation by on-line electrochemistry/electrospray ionization mass spectrometry, J. Am. Soc. Mass Spectrom. 15 (2004) 1228–1236.
[40] S.K. Trabelsi, N.B. Tahar, R. Abdelhedi, Electrochemical behavior of caffeic acid, Electrochim. Acta 49 (2004) 1647–1654.
[41] S.C. Mordido, M.J.F. Rebelo, Electrochemistry of caffeic acid in acetate–ethanolic solutions, Port. Electrochim. Acta 24 (2006) 313–322.
[42] B.L. Zeller, W.W. Kaleda, F.Z. Saleeb, US Pat. 4,521,438, Patented, 1985.
[43] J.L. Beltran, N. Sanli, G. Fonrodona, D. Barron, G. Ozkan, J. Barbosa, Spectrophotometric potentiometric and chromatographic p*Ka* values of polyphenolic acids in water and acetonitrile–water media, Anal. Chim. Acta 484 (2003) 253–264.
[44] C.C. Zeng, L.M. Hu, J. Zeng, R.G. Zhong, A facile electrochemical synthesis of caffeic acid derivatives in the presence of acetylacetone or methyl acetoacetate, Chin. Chem. Lett. 18 (2007) 130–132.
[45] V.L. Singeton, Oxygen with phenols and related reactions in musts, wines, and model systems: observations and practical implications, Am. J. Enol. Vitic. 38 (1987) 69–77.
[46] J.J.L. Cilliers, V.L. Singleton, Characterization of the products of nonenzymic autoxidative phenolic reactions in a caffeic acid model system, J. Agri. Food Chem. 39 (1991) 1298–1303.
[47] H. Lund, O. Hammerich, Organic Electrochemistry, fourth ed., Marcel Dekker, New York, 2001 (Chapter 8).
[48] N. Takeda, P.V. Poliakov, A.R. Cook, J.R. Miller, Faster dissociation: measured rates and computed effects on barriers in aryl halide radical anions, J. Am. Chem. Soc. 126 (2004) 4301–4309.
[49] A.A. Isse, S. Gottardello, C. Durante, A. Gennaro, Dissociation electron transfer to organic chlorides: electrocatalysis at metal cathods, Phys. Chem. Chem. Phys. 10 (2008) 2409–2416.
[50] A.A. Isse, P.R. Mussini, A. Gennaro, New insight into electrocatalysis and dissociative electron transfer mechanisms: the case of aromatic bromides, Phys. Chem. Chem. Phys. 10 (2008) 2409–2416.
[51] D.O. Wipf, R.M. Wightman, Rapid cleavage reactions of haloaromatic radical anions measured with fast-scan cyclic voltammetry, J. Phys. Chem. 93 (1989) 4286–4291.
[52] H. Jensen, K. Daasbjerg, Solvent effects on the reduction mechanism of 9-chloroanthracene, 3-nitrobenzyl chloride and 3-chloroacetophenone, Acta Chem. Scand. 52 (1998) 1151–1164.
[53] A.A. Isse, L. Falciola, P.R. Mussini, A. Gennaro, Relevance of electron transfer mechanism in electrocatalysis: the reduction of organic halides at silver electrodes, Phys. Chem. Chem. Phys. 10 (2008) 2409–2416.
[54] J.M. Saveant, Electron transfer bond breaking and bond formation, Adv. Phys. Org. Chem. 35 (2000) 117–192.
[55] L. Nadjo, J.M. Saveant, Linear sweep voltammetry: kinetic control by charge transfer and/or secondary chemical reactions: I. Formal kinetics, J. Electroanal. Chem. 48 (1973) 113–145.
[56] H. Lund, A century of organic electrochemistry, J. Electrochem. Soc. 149 (2002) S21–S33.